Alzheimer's Research & Therapy

RESEARCH

Open Access

Fibre density and cross-section associate with hallmark pathology in early Alzheimer's disease

Greet Vanderlinden[1*], Ahmed Radwan[2], Daan Christiaens[2], Jeroen Blommaert[3], Stefan Sunaert[2,4,5], Mathieu Vandenbulcke[5,6,7], Michel Koole[1] and Koen Van Laere[1,5,8]

Abstract

Background Tau pathology in Alzheimer's disease (AD) propagates trans-synaptically along structurally connected brain networks and in synergy with amyloid pathology it induces synaptic damage. However, the in vivo relationship of amyloid, tau and synaptic density with white matter (WM) structural changes has been studied rather limitedly. Recent advances in diffusion MRI processing allow quantification of apparent fibre density and fibre cross-section on the fixel level, i.e., individual fibre populations within one voxel. The aim of this study was to investigate the hypothesis of axonal loss due to tau propagation and amyloid pathology and its association with synaptic density in early disease stages.

Methods Twenty-four patients with amnestic mild cognitive impairment (aMCI) and 23 healthy controls (HC) underwent baseline amyloid (^{11}C-PiB/^{18}F-NAV4694), tau (^{18}F-MK-6240) and synaptic density (^{11}C-UCB-J binding to SV2A) PET/MR in combination with diffusion MRI and cognitive assessments. A subset of 14 aMCI patients underwent follow-up visits after 2 years. First, a whole-brain fixel-based analysis was performed to identify differences in fibre density and fibre cross-section between HC and aMCI and longitudinally in the aMCI group. Next, a tract-of-interest analysis was performed, focusing on the temporal-cingulum bundle where most alterations have been shown in early AD. Tau and SV2A PET were quantified in the connected regions, i.e., hippocampus and posterior cingulate/precuneus (PCC-P). Amyloid PET centiloids were measured in the commonly used cortical composite volume-of-interest.

Results At baseline, multiple WM tracts showed lower fibre density and lower fibre cross-section in aMCI compared to HC, and these parameters further decreased longitudinally in the aMCI group. In the temporal cingulum bundle, reduced fibre density was significantly associated with reduced hippocampal synaptic density while increased hippocampal and PCC-P tau specifically correlated with reduced fibre cross-section. Increased global amyloid burden was associated with reduced fibre density and fibre cross-section in the temporal cingulum bundle.

Conclusions Our results suggest that WM degeneration already occurs in the aMCI stage of AD and alterations in apparent fibre density and fibre cross-section of the temporal cingulum bundle are associated with AD hallmark pathology.

*Correspondence:
Greet Vanderlinden
Greet.vanderlinden@kuleuven.be

Full list of author information is available at the end of the article

Keywords Diffusion MRI, Fixel-based analysis, Mild cognitive impairment, Tau, Synaptic density, Amyloid

Background

Alzheimer's disease (AD) is characterized by the accumulation of amyloid-β (Aβ) plaques that spread from the neocortex to the mesiotemporal cortex [1, 2]. A second AD hallmark is the deposition of tau neurofibrillary tangles (NFTs) that starts in the (trans)entorhinal cortex, spreading first to other mesiotemporal brain regions such as the hippocampus and parahippocampal gyrus, before migrating towards neocortical areas [1]. In early disease stages, Aβ plaques induce functional network hyperexcitability [3–5] and facilitate the trans-synaptic spread of pathological tau out of the mesiotemporal cortex into neocortical brain regions [6–11]. Tau binding to presynaptic vesicles causes presynaptic dysfunction by lowering neurotransmission and ultimately results in synaptic loss [12, 13]. As the disease progresses and pathological tau is propagated along brain networks [14, 15], functional as well as structural network connectivity starts to decrease [16–18]. This network disconnection in AD has been confirmed by functional MRI studies [16, 19, 20]. Moreover, the analysis of the underlying structural connections has been performed by diffusion tensor imaging (DTI). Using this technique, Vogel et al. showed that highly connected regions are affected sooner by tau pathology along a structural network starting from the mesiotemporal cortex [9]. Additionally, DTI has been used to quantify fractional anisotropy (FA) and mean diffusivity (MD) as indications of white matter (WM) structure. Many studies have shown widespread FA decreases as well as MD increases in both patients with mild cognitive impairment (MCI) and AD [21–24]. Some studies have also demonstrated a relationship of these WM structural changes with Aβ plaque and tau NFT load [25–31]. However, a crucial shortcoming of DTI is its inability to account for crossing fibres within WM voxels. As most of the brain's WM voxels contain crossing fibres [32], the physiological interpretation of FA and MD measures is not entirely straightforward [33]. To overcome this, constrained spherical deconvolution (CSD) has been proposed for processing of diffusion-weighted magnetic resonance images (dMRI) to obtain fibre orientation distribution functions [34]. This method can tackle the problem of crossing fibres and can detect specific fibre bundles within a voxel (i.e. fixels) [35]. Correspondingly, measures of apparent fibre density (FD), fibre cross-section (FC) or a combination of both apparent fibre density and cross-section (FDC) can be derived from a fixel-based analysis (FBA) to investigate microstructural (FD) and macroscopic (FC) differences in WM bundles [35].

Recent studies have focused on this fixel-based approach to study WM structural changes in MCI and AD. Mito et al. [36] identified the temporal cingulum bundle as the only WM bundle with decreased FDC in MCI whereas patients with AD showed decreased FDC in many more tracts, with largest effect sizes in the posterior parietal WM and parahippocampal aspect of the cingulum bundle. Giraldo et al. [37] demonstrated decreased FD and FC in the splenium, cingulum and longitudinal fasciculi in a combined cohort of AD and MCI compared to cognitively unimpaired subjects. However, longitudinal evaluations of FD, FC and FDC have not been investigated and their associations with tau, amyloid, synaptic density and cognition remain elusive.

In this work, we aimed to investigate the hypothesis that spreading of pathological tau through WM bundles in the presence of amyloid pathology would be associated with WM micro- and macrostructural alterations that are also related to loss of synaptic density. Therefore, we first assessed to what extent WM micro- and macrostructural alterations were present in our cohort. We evaluated FD, FC and FDC in a whole-brain FBA, both cross-sectionally comparing patients with amnestic MCI (aMCI) versus healthy controls (HC), as well as longitudinally within the cohort of aMCI patients over a 2-year follow-up period. Second, we performed a tract-of-interest analysis, focusing on the temporal cingulum bundle that connects the hippocampus and posterior cingulate cortex/precuneus, both of which are regions implicated in early tau pathology [38] and synaptic loss [39]. This enabled the investigation of our study hypothesis evaluating the relationship of mean FD, FC and FDC across the temporal cingulum bundle with tau and synaptic density PET measures in the adjacent brain regions and with cerebral amyloid load.

Methods

Participants

Eligible patients were diagnosed with aMCI according to the clinical Albert criteria [40], and were referred by a neurologist or psychiatrist from the tertiary memory clinic of the Leuven University Hospital or from an independent neurology practice specialized in dementia between April 2018 and December 2021. All patients had a clinical dementia rating (CDR) score of 0.5 at inclusion. HC between 50 and 85 years old were recruited through local newspapers and internet advertisements. Physical and mental health was thoroughly assessed by urine and blood analysis as well as by neuropsychological testing. Exclusion criteria for HC were history of major neurologic, psychiatric or internal pathology, history of alcohol or other drug abuse and MR abnormalities including brain white matter disease Fazekas

3. All subjects underwent cognitive screening covering domains of global cognition (Mini-Mental State Examination (MMSE)), memory (Rey Auditory Verbal Learning test (RAVLT)), attention and executive functioning (Trail Making Test (TMT) A and B, animal verbal fluency (AVF) and Raven's coloured progressive matrices (RCPM)) and language (Boston Naming Test (BNT)). Depressive symptoms were assessed using the Beck Depression Inventory (BDI) and the Geriatric Depression Scale (GDS). All cognitive screening tests were repeated in aMCI patients at the 2-year follow-up study visits.

The study was approved by the local Ethics Committee UZ/KU Leuven and was conducted according to the latest version of the Declaration of Helsinki. Written informed consent was signed by all participants prior to study inclusion. This study is part of a larger, multimodal, multitracer imaging study which also included other patient populations (on ClinicalTrials.gov since 2018-05-02 as NCT03514524). Tau and synaptic vesicle 2 A (SV2A) PET data in a subset of this study population have been published previously [39].

Image acquisition

PET tracers were synthesized as previously described [41, 42]. All participants underwent a 30-min ^{18}F-MK-6240 PET-MR (tau), acquired 90–120 min post-injection (injected activity 142±24 MBq) and a 30-min ^{11}C-UCB-J PET-MR (synaptic density), acquired 60–90 min post-injection (injected activity 221±65 MBq). All scans were performed on an integrated timeofflight 3T PET-MR scanner (Signa, GE Healthcare, Milwaukee, WI, USA). Participants also underwent an amyloid ^{18}F-NAV4694 or ^{11}C-Pittsburgh compound B (^{11}C-PiB) PET scan on the same PET-MR scanner or on a PET-CT scanner (Biograph TruePoint, Siemens, Erlangen, Germany), respectively.

^{18}F-MK-6240 and ^{11}C-UCB-J PET acquisitions were rebinned into 6 frames of 5 min and reconstructed using an ordered subset expectation maximization (OSEM) algorithm (4 iterations and 28 subsets), with corrections for scatter, random coincidences, deadtime and radioactive decay. Attenuation correction was zero-echo time (ZTE) MR-based as reported previously [43]. Three-dimensional isotropic 4 mm Gaussian smoothing was applied to reduce image noise. ^{18}F-NAV4694 and ^{11}C-PiB scans were reconstructed using VPFXS and OSEM algorithms (2 iterations and 32 subsets for ^{18}F-NAV4694 and 3 iterations and 21 subsets for ^{11}C-PiB) and 3D isotropic 4.5 mm and 2 mm Gaussian smoothing was applied, respectively.

Simultaneously with the ^{18}F-MK-6240 or ^{11}C-UCB-J PET, a 3D T1-weighted MRI (plane: sagittal; TE: 3.2 ms; TR: 8.5 ms; TI: 450 ms; flip angle: 12°; 1 mm isotropic voxels; acquisition matrix: $166 \times 256 \times 256$) and multi-shell dMRI (plane: axial; TE: 86 ms; TR: 10.34 s; flip angle 90°; 2.5 mm isotropic voxels; phase encoding: RL; b-values: 0/700/1000/2000 s/mm^2 with 16/20/32/66 uniformly distributed gradient directions respectively; acceleration factor (ASSET): 2; acquisition matrix: $96 \times 96 \times 48$) were acquired using a vendorsupplied 8-channel brain phased array head coil. aMCI patients underwent 2-year follow-up ^{18}F-MK-6240 and ^{11}C-UCB-J PET scans as well as T1-weighted MRI and dMRI scans, all acquired using the same scanning protocols and same head coil on the same scanner that was used for baseline acquisitions.

Image analysis

PET

Reconstructed PET images were corrected for motion with PMOD software (v4.1, PMOD Inc. Zurich, Switzerland), using a rigid frame by frame co-registration to the first frame. Subsequently, all motion-corrected frames were averaged, and this mean image was rigidly co-registered to the corresponding T1-weighted MRI of the corresponding timepoint. The CAT12 toolbox of SPM12 (Statistical Parametric Mapping, Wellcome Trust Centre for Neuroimaging, University College, London, UK) was used for segmentation of T1-weighted MRI and hippocampus and posterior cingulate/precuneus (PCC-P) volumes-of-interest (VOIs) were delineated according to the Neuromorphometrics atlas. The rationale for quantifying a combined PCC-P VOI came from the pipeline that was used for segmenting the temporal cingulum bundle, which also includes both posterior cingulum and precuneus as inclusion VOIs for delineation of the tract [44]. A region-based voxelwise (RBV) partial volume correction (PVC) was applied to the standardized uptake value (SUV) maps for ^{18}F-MK-6240 and ^{11}C-UCB-J [45], where the PET resolution was modelled as a 3D isotropic Gaussian kernel with a full width at half maximum (FWHM) of 5 mm. All cortical VOIs as defined by the Neuromorphometrics atlas were provided individually as input for the RBV while white matter VOIs and cerebrospinal fluid (CSF) VOIs were merged to obtain one VOI for whiter matter and one VOI for CSF. For ^{18}F-MK-6240, cortical VOIs as obtained from the Neuromorphometrics atlas were merged unilaterally into composite VOIs for the frontal, temporal, parietal, mesotemporal and occipital cortex to assure robustness of the PVC algorithm. Next, SUV ratios (SUVR) were calculated using the inferior cerebellar cortex for ^{18}F-MK-6240 and centrum semiovale for ^{11}C-UCB-J [46, 47]. For the voxel-based analyses, SUVR maps were spatially normalized to Montreal Neurological Institute (MNI) space using a non-linear registration as obtained by the CAT12 toolbox of SPM12 and smoothed using an isotropic Gaussian

kernel with 8 mm FWHM (voxel size: 1.5 mm x 1.5 mm x 1.5 mm).

Amyloid ^{18}F-NAV4694 and ^{11}C-PiB SUVR were calculated using the cerebellar cortex as a reference region which was defined by the automated anatomical labelling (AAL) atlas (regions 91–108). The mean SUVR was calculated in a composite VOI consisting of bilateral frontal (AAL areas 3–10, 13–16, 23–28), parietal (AAL 57–70) cingulate (AAL 31–32 and 35–36) and lateral temporal cortices (AAL 81–82, 85–90) and converted to centiloids using the formula: $CL = 132.53 \times SUVR_{comp}$ -147.64 for ^{11}C-PiB and $CL = 107.78 \times SUVR_{comp} - 114.71$ for ^{18}F-NAV4694, both validated in-house (not previously published). Amyloid PET scans were not corrected for partial volume effects. Additionally, amyloid PET scans were visually classified as being positive or negative by an expert reader (K.V.L.).

Diffusion MRI

Pre-processing of the diffusion-weighted images was performed using MRtrix3 software [48, 49] that included denoising [50], and corrections for Gibbs ringing [51], subject motion, EPI distortion [52] and intensity bias field [53]. Afterwards, data were up-sampled to an isotropic resolution of 1.3 mm. Using multi-shell, multi-tissue constrained spherical deconvolution [54], fibre orientation distributions (FODs) were calculated for each subject separately and at both timepoints for aMCI patients.

Fixel-based analysis For cross-sectional FBA, a study-specific baseline WM FOD template was created from 30 included subjects (15 HC and 15 aMCI) and all subject-specific WM FODs were registered to this template using a non-linear registration as obtained by the mrregister command in MRtrix3. A whole-brain tractogram was created on this population template where first 20 million streamlines were generated, which were then filtered to 2 million streamlines by the SIFT algorithm [55, 56]. Finally, measures of FD, FC and FDC were computed for each subject. More specifically, FD was calculated as the apparent fibre density in the FOD lobe and FC was measured by the relative inter-subject deformation field. A more detailed description of these measures can be found in Raffelt et al. [35]. As recommended in the FBA pipeline, the FC maps were log-transformed and measures of FC reported throughout the paper are thus log-transformed FC values.

For longitudinal FBA in the aMCI group, a previously published workflow was followed [57]. First, we created intra-subject templates using the WM FODs from the two timepoints. WM FODs from both timepoints were then rigidly registered to the intra-subject template. Afterwards, a group- or inter-subject template was created from all intra-subject templates and the WM FODs were non-linearly warped to the final group template. As for the cross-sectional FBA, a whole-brain tractogram with 20 million streamlines was then created from this longitudinal population template and SIFT filtered to 2 million streamlines after which FD, FC and FDC were computed.

Tract-of-interest analysis Similar to the creation of the WM FOD template, a study-specific baseline T1-weighted baseline MRI template was created which was used for parcellation by Freesurfer v6.0 and the MultiScale Brain Parcellator (MSBP) to obtain Volumes-Of-Interest (VOIs). Using these VOIs as in- and exclusion regions, the dissection pipeline FWT was used to isolate the temporal cingulum bundle as a tract-of-interest [44]. Supplementary Fig. 1 shows the dissection of the temporal cingulum bundle.

Statistical analysis

General statistical analyses were performed in GraphPad Prism version 9 (GraphPad Software, La Jolla, CA). Data are presented as mean ± standard deviation (SD) unless otherwise specified. Normality of the data distributions was assessed by Shapiro-Wilk tests ($\alpha = 0.05$). Demographic characteristics were compared between groups using an unpaired Student t-test, unpaired Mann-Whitney U-test, Fischer's exact test, Chi-square test or Chi-square test for trend as appropriate ($\alpha = 0.05$).

PET voxel-based group comparisons were performed using an unpaired t-test in SPM with thresholds for cluster height and voxel height of $P_{FWE} < 0.05$ and $P_{uncorrected} < 0.001$, respectively. To exclude extracerebral clusters, a binary grey matter mask was applied. For correlation analyses, mean SUVR was calculated in the hippocampus and in a combined VOI of the posterior cingulate cortex and the precuneus.

For dMRI analyses, FD, FC and FDC of each fixel were compared in a general linear model between HC and aMCI patients at baseline. For longitudinal changes in the aMCI group, difference images were calculated for FD, FC and FDC by subtracting the timepoint 2 image from the timepoint 1 image and statistical inferences were performed on these difference images. For all FC and FDC analyses, total intracranial volume (TIV) was included as a nuisance covariate [58]. Images were smoothed using a connectivity-based smoothing with default smoothing parameters (10 mm full-width at half-maximum). Next, statistical inference was performed using a connectivity-based fixel enhancement (CFE) approach [59]. This provides family-wise error (FWE) corrected *P*-values for all individual fixels, based on non-parametric permutation testing over 5000 permutations. For longitudinal FBA, shuffling of independent and symmetric errors was performed through sign-flipping [60]. Significant

fixels (P_{FWE} < 0.05) were displayed as streamline segments on the group template and color-coded by streamline orientation (left-right = red; inferior-superior = blue; anterior-posterior = green).

For the tract-of-interest analysis, mean FD, FC and FDC were calculated using the isolated temporal cingulum bundle streamlines as a mask. Group comparisons of FD, FC and FDC in the temporal cingulum bundle were performed using an unpaired Student t-test for baseline comparisons, and a Paired student t-test for longitudinal comparisons. Correlations of baseline dMRI metrics in the temporal cingulum bundle with baseline PET outcomes were performed in the combined cohort of aMCI patients and HC using Pearson or Spearman correlations as appropriate. These analyses were performed on a significance level of α = 0.05 without correction for multiple comparisons due to the exploratory character.

Results

Clinical characteristics

A total of 26 HC and 30 aMCI patients underwent baseline ^{18}F-MK-6240 and ^{11}C-UCB-J PET scans of which 21 aMCI patients also underwent 2-year follow-up PET scans. dMRI was successfully acquired in a subset of 23 HC and 24 aMCI patients at baseline and in 14 aMCI patients at 2-year follow-up. All study analyses were performed on this cohort for which ^{18}F-MK-6240, ^{11}C-UCB-J PET and dMRI scans were available. Demographics of this cohort are shown in Table 1. Age and sex were not significantly different between the HC and aMCI groups. Amyloid PET was acquired at baseline for all participants except for one aMCI patient who terminated his study participation early. Based on visual assessments, the prevalence of amyloid positivity was higher in the aMCI group compared to the HC group ($P < 0.0001$). MMSE and RAVLT scores were significantly lower in aMCI compared to HC at baseline (both $P < 0.0001$) and a significant longitudinal decline was present for both test scores in the aMCI group (MMSE: $P = 0.04$; RAVLT: $P = 0.03$). Time between baseline and follow-up tau and synaptic density PET was 25 ± 1 months (range: 23–28 months) for both.

White matter structure

FD was significantly lower in aMCI patients compared to HC in the fornix and the splenium of the corpus callosum (Fig. 1A). FC was also significantly lower in aMCI patients compared to HC in parts of the temporal cingulum bundle, parts of the inferior longitudinal fasciculus, and in parts of the uncinate fasciculi (Fig. 1B). FDC was significantly lower in aMCI patients compared to HC in parts of the temporal and cingulate cingulum bundle, in parts of the inferior longitudinal fasciculus and in the fornix and splenium of the corpus callosum (Fig. 1C). Since FDC and FC were significantly reduced in the temporal cingulum bundle, and this bundle connects early tau accumulating regions [39], we isolated this tract using the FWT pipeline [44]. In the temporal cingulum bundle, FD was lower in aMCI patients compared to HC in the

Table 1 Demographical and clinical characteristics of included participants

Variable	HC	aMCI		*P*-value	
		Baseline	Follow-up	HC vs. MCI_{Base}	MCI_{Base} vs. MCI_{FU}
N	23	24	14		
Age, y	70 ± 9	73 ± 8	72 ± 8	0.3	N.A.
Sex (F/M), n	10/13	15/9	8/6	0.2	N.A.
Education, n				**0.04**	N.A.
Secondary education	4	13	8		
Higher education	15	8	5		
University	4	3	1		
APOEε4 alleles (0/1/2), n	18/3/2	6/13/5	3/8/3	**0.002**	N.A.
Aβ (+/-/unknown), n	4/19/0	23/0/1	14/0/0	**< 0.0001**	N.A.
MMSE (0–30)	29.5 ± 0.8	25.2 ± 2.2	22.6 ± 2.6	**< 0.0001**	**0.03**
RAVLT Sum (0–75)	53.3 ± 9.0	29.0 ± 9.8	22.7 ± 5.5	**< 0.0001**	**0.04**
RCPM (0–24)	21.7 ± 2.0	17.6 ± 3.6	15.9 ± 4.5	**< 0.0001**	**0.007**
AVF	25.4 ± 7.4	14.9 ± 4.3	13.2 ± 3.1	**< 0.0001**	0.2
BNT (0–60)	56.2 ± 3.4	50.2 ± 7.6	48.2 ± 6.3	**< 0.0001**	**0.001**
TMT, s					
TMT A	33.4 ± 12.1	57.0 ± 23.6	48.0 ± 15.7	**< 0.0001**	0.6
TMT B	83.1 ± 75.7	179.3 ± 76.3	163.9 ± 43.0	**< 0.0001**	0.2
BDI (0–63)	3.6 ± 3.2	6.9 ± 5.7	6.2 ± 4.4	**0.02**	0.8
GDS (0–30)	2.7 ± 2.6	8.7 ± 5.7	8.0 ± 4.2	**< 0.0001**	0.1

Data are presented as mean ± SD. Significant findings are indicated in bolt. GDS and BDI were missing for one HC, baseline TMT A was missing for one aMCI and baseline TMT B was missing for two aMCI patients. Follow-up TMT A and B as well as BDI were missing in one aMCI patient. Aβ = amyloid-beta PET status; aMCI = amnestic mild cognitive impairment; Base = baseline; FU = follow-up; HC = healthy controls; MMSE = mini-mental state examination; N.A. = not applicable; RAVLT = Rey auditory verbal learning test

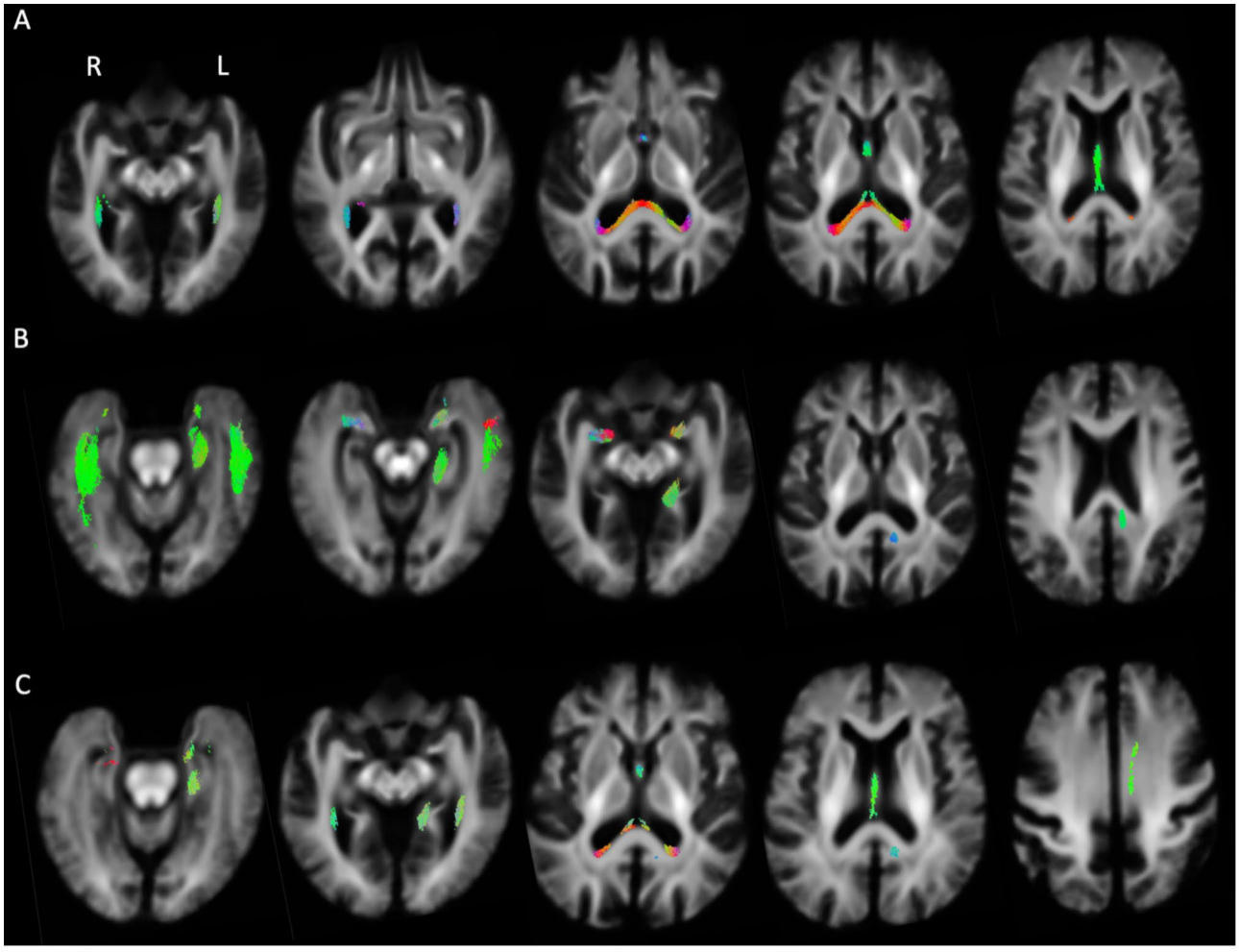

Fig. 1 Cross-sectional whole-brain fixel-based analysis. (**A**) Decreased fibre density, (**B**) fibre cross-section and (**C**) fibre density and cross-section in aMCI patients compared to HC. Results are shown as streamline segments traversing fixels (P_{FWE}<0.05) and coloured by diffusion direction: red = right-left; green = anterior-posterior; blue = inferior-superior. Images are shown in radiological convention. aMCI = amnestic mild cognitive impairment; HC = healthy controls

left hemisphere ($t = 3.01$, $P = 0.004$) and in the right hemisphere ($t = 3.00$, $P = 0.004$). FC was also lower in aMCI patients compared to HC in the left hemisphere ($t = 3.2$, $P = 0.004$) and in the right hemisphere ($t = 2.0$, $P = 0.05$). FDC was lower in aMCI patients compared to HC in the left hemisphere ($t = 3.8$, $P = 0.0004$) and in the right hemisphere ($t = 3.3$, $P = 0.002$).

Longitudinally, the whole-brain FBA in the aMCI group showed fixels with significantly reduced FD in the fornix and splenium of the corpus callosum (Fig. 2A). FC was significantly reduced in the temporal and cingulate cingulum bundle, in parts of the superior and inferior longitudinal, and in parts of the left inferior fronto-occipital fasciculi (Fig. 2B). FDC was significantly reduced in a posterior part of the inferior fronto-occipital fasciculus, in the splenium of the corpus callosum, fornix and in parts of the inferior longitudinal fasciculus (Fig. 2C). As for longitudinal structural changes in the temporal cingulum bundle, FD further decreased significantly in the left hemisphere ($t = 2.7$, $P = 0.02$) but not in the right hemisphere ($t = 1.6$, $P = 0.1$) in the aMCI group. Longitudinal FDC and FC decreases were significant in both the left (FDC: $t = 3.6$, $P = 0.003$; FC: $t = 6.5$, $P < 0.0001$) and right (FDC: $t = 2.2$; $P = 0.04$; FC: $t = 3.0$, $P = 0.01$) hemisphere.

Amyloid, tau and synaptic density PET

Amyloid load was significantly higher in aMCI patients compared to HC in all grey matter regions (Fig. 3A) whereas tau was significantly higher in medial temporal regions, posterior cingulate, precuneus, frontal and lateral temporal regions (Fig. 3B). Synaptic density was significantly lower in aMCI patients compared to HC in the right medial temporal cortex (Fig. 3C). These results are consistent with our pilot study that included a subset

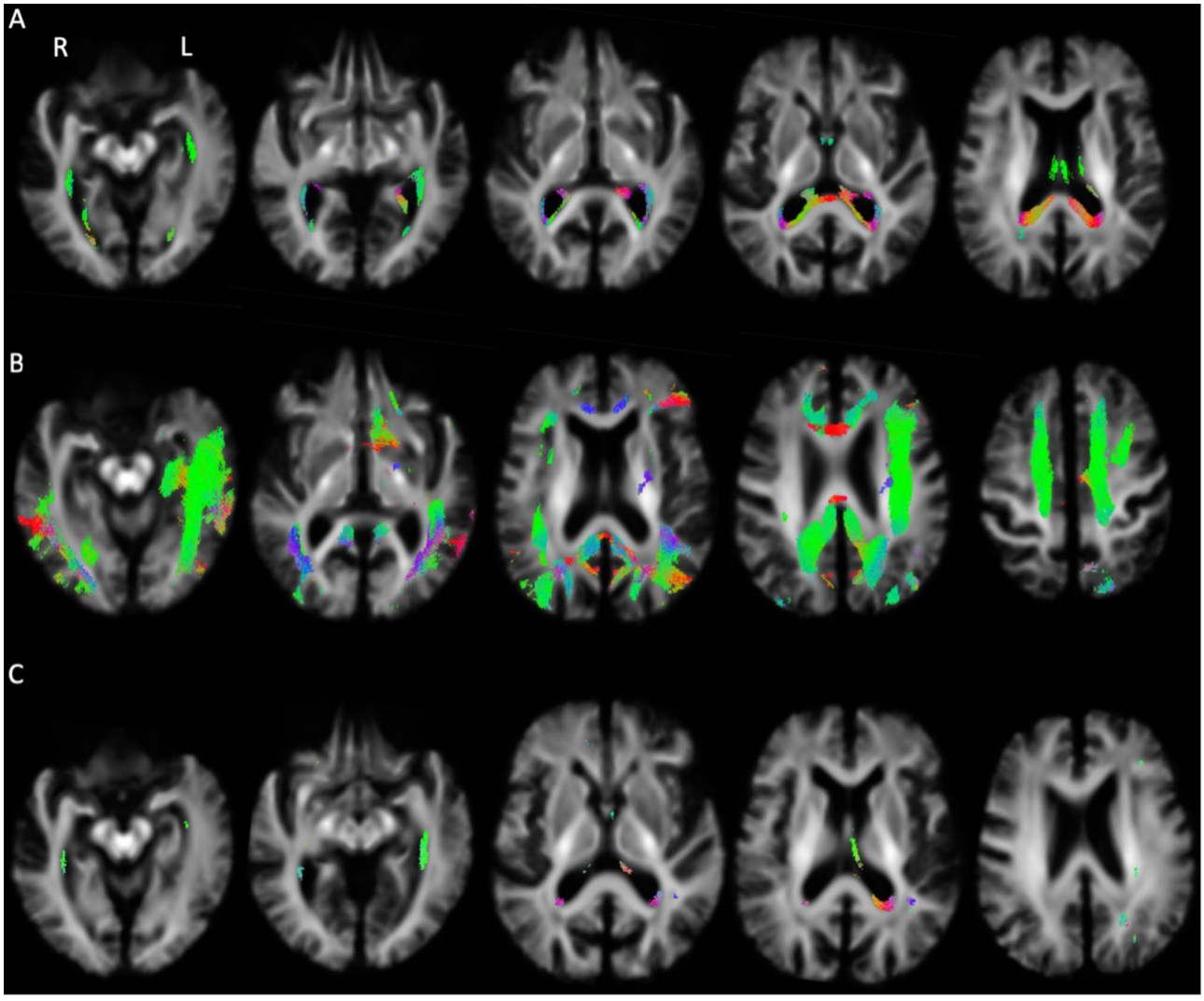

Fig. 2 Longitudinal whole-brain fixel-based analysis. (**A**) Decreased fibre density, (**B**) fibre cross-section and (**C**) fibre density and cross-section in aMCI patients at follow-up compared to baseline. Results are shown as streamline segments traversing fixels (P_{FWE}<0.05) and coloured by diffusion direction: red = right-left; green = anterior-posterior; blue = inferior-superior. Images are shown in radiological convention. aMCI = amnestic mild cognitive impairment

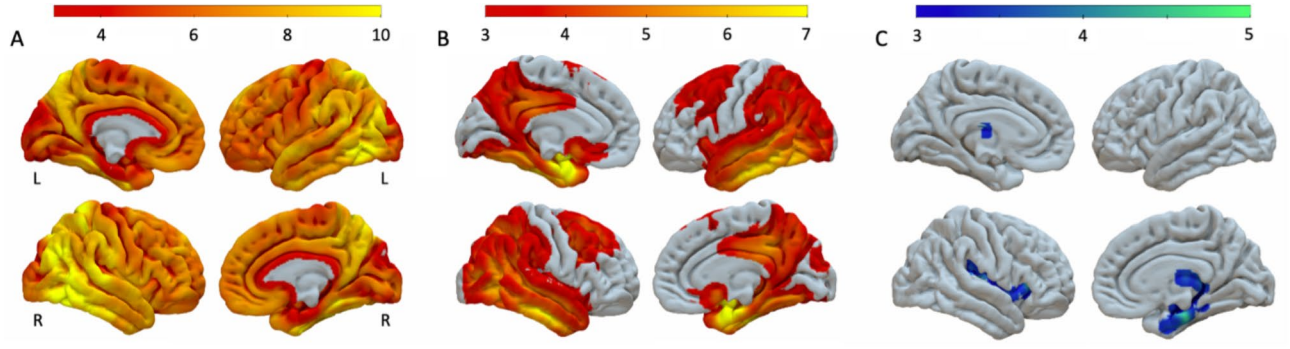

Fig. 3 Voxel-based group comparisons. Clusters of significantly (**A**) increased amyloid PET, (**B**) increased tau PET and (**C**) reduced synaptic density PET in aMCI compared to HC. Colour bars indicating SPM t-values. Thresholds for cluster height and voxel height were $P_{FWE} < 0.05$ and $P_{uncorrected} < 0.001$, respectively. aMCI = amnestic mild cognitive impairment; HC = healthy controls; PET = positron emission tomography; SPM = statistical parametric mapping

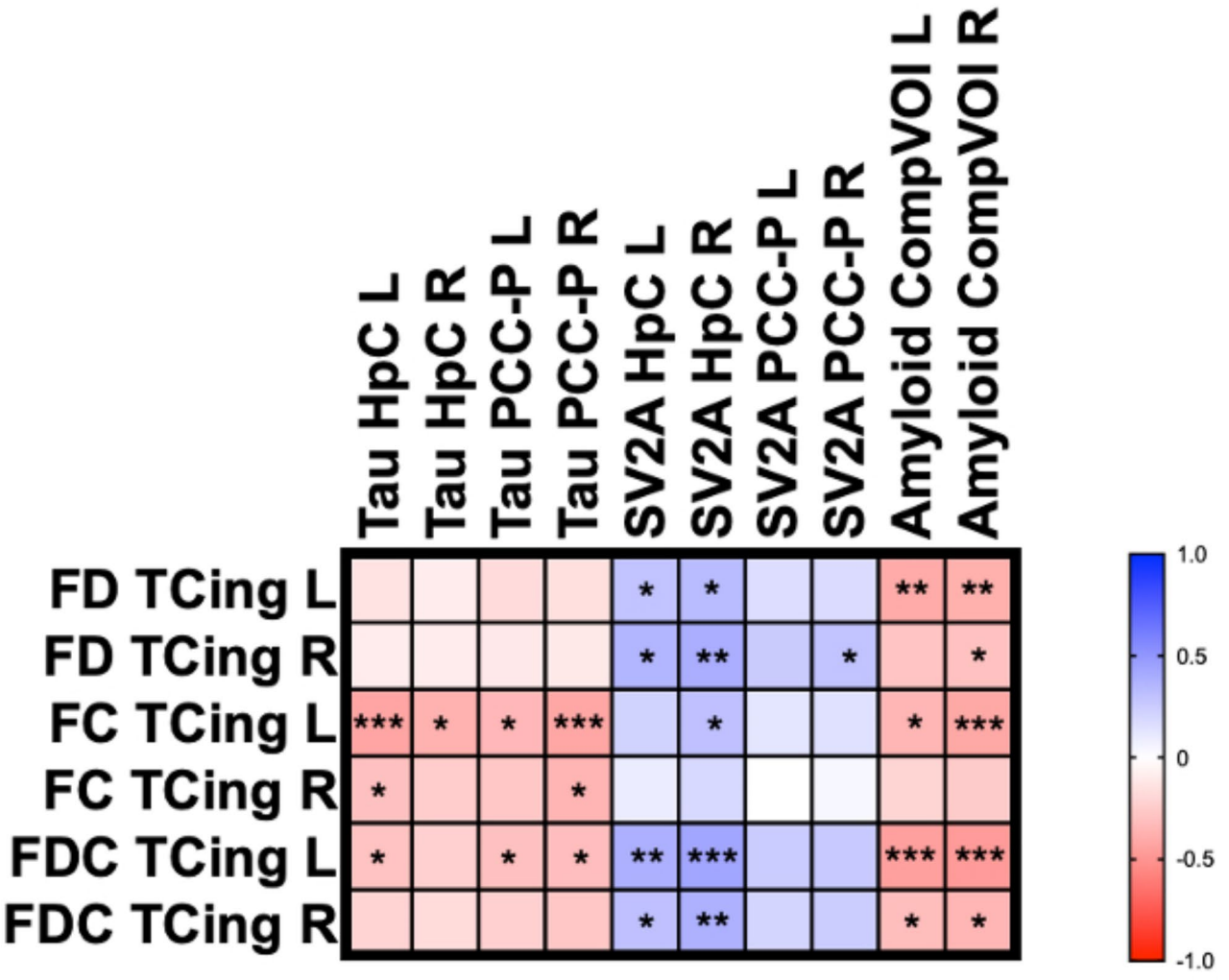

Fig. 4 Association of temporal cingulum fixel metrics with PET biomarker findings. The correlation matrix is coloured by Spearman correlation coefficients and significance is indicated by $^{*}P < 0.05$, $^{**}P < 0.01$, $^{***}P < 0.005$, uncorrected for multiple comparisons. CompVOI = composite volume-of-interest; FC = fibre cross-section; FD = fibre density; FDC = fibre density and cross-section; HpC = hippocampus; PCC-P = posterior cingulate cortex and precuneus; L = left; R = right

of this study cohort [39] and are reported in more detail elsewhere for the full cohort [61].

Correlation of PET biomarkers with white matter structure

In the full set of aMCI and HC subjects, baseline temporal cingulum FD correlated significantly with baseline hippocampal synaptic density (left: r_p = 0.29, $P = 0.05$; right: r_p = 0.37, $P = 0.01$) but no significant associations were found with hippocampal tau, PCC-P tau, nor with PCC-P synaptic density (all $P > 0.1$). FD in the temporal cingulum bundle was also significantly associated with amyloid as quantified in the composite VOI (left: r_s = -0.40, $P = 0.006$; right: r_s = -0.30, $P = 0.04$). In contrast, temporal cingulum FC was not significantly associated with hippocampal nor PCC-P synaptic density (all $P > 0.1$). However, it did correlate significantly with hippocampal tau in the left but not right hemisphere (left: r_s = -0.43, $P = 0.003$; right: r_s = -0.25, $P = 0.09$). Additionally, FC was significantly associated with PCC-P tau (left: r_s = -0.34, $P = 0.02$; right: r_s = -0.36, $P = 0.01$) and also with amyloid in the left but not right hemisphere (left: r_s = -0.35, $P = 0.02$; right: r_s = -0.26, $P = 0.08$). FDC was significantly associated with hippocampal tau in the left but not right hemisphere (left: r_s = -0.29, $P = 0.05$; right: r_s = -0.18, $P = 0.23$) and with PCC-P tau in the left but not right hemisphere (left: r_s = -0.30, $P = 0.04$; right: r_s = -0.28, $P = 0.06$). Moreover, FDC was significantly associated with hippocampal SV2A (left: r_p = 0.34, $P = 0.02$; right: r_p = 0.35, $P = 0.02$) but not with PCC-P SV2A (both $P > 0.05$). Finally, FDC was significantly associated with amyloid (left: r_s = -0.45, $P = 0.002$; right: r_s = -0.35, $P = 0.02$). These results are summarized in Fig. 4 and individual correlation plots are shown in Supplementary Figs. 2–4.

Discussion

In this prospective longitudinal cohort study, we quantified WM micro- and macrostructural changes cross-sectionally in aMCI patients versus HC and longitudinally over 2 years in aMCI patients. We also assessed correlations of WM structural changes with AD hallmark pathology as measured by amyloid, tau and SV2A PET. The main findings of our study are that (i) FD, FC and FDC are reduced already in the aMCI stage of AD when compared to HC; (ii) FD, FC and FDC further decrease longitudinally and extensively along multiple fibre bundles; and (iii) FD reduction was associated with hippocampal SV2A loss while FC reduction was associated with both hippocampal and PCC-P tau pathology.

Cross-sectionally, FC and FDC were both reduced in the temporal cingulum bundle. This result in aMCI patients is consistent with previous FBA findings in AD [36, 37, 62, 63]. While the microstructure of the tract (FD) did not change significantly, morphological atrophy as measured by FC was statistically significant and spatially extensive. In contrast to our findings, Mito et al. [36]. found no significant difference in a whole-brain FBA in MCI versus HC, although a tract-of-interest analysis showed significantly decreased FDC in the left temporal cingulum bundle. In our study, all patients (except for one with unknown amyloid status) were positive for amyloid PET, indicating that they are on the AD continuum. Moreover, next to FDC, we investigated FD and FC individually in contrast to comparing only FDC value between groups. Next to the whole-brain FBA, our tract-of-interest findings confirm that the temporal cingulum bundle is affected in early disease stages. This is in line with previous voxel-based DTI findings [25]. In early disease stages, the hippocampus and posterior cingulate cortex/precuneus, connected by the temporal cingulum bundle, show hypometabolism [64, 65] and functional disconnection [66] as a result of AD pathology, although hypometabolism shows considerable variability in medial temporal regions [67]. In addition, the temporal cingulum bundle is part of the Papez circuit that is associated with memory formation and changes in the functional connectivity of the Papez circuit along the AD continuum have been shown previously [17]. With this study, we provide evidence for WM structural changes underlying this functional disruption.

Longitudinal analyses showed further reductions in FD, FC and FDC within the aMCI group. Nonetheless, differences concerning the specifically affected bundles and the spatial extent as to which they are affected, were present. Interestingly, we found longitudinal reductions in FD mostly in short association fibres whereas FC was reduced in long association fibres. The more extensive reductions found in FC, a marker of macroscopic change, compared to those found on FD, a marker of microscopic change, indicate that axonal density loss in AD predominantly manifests as bundle atrophy rather than microscopic rarefaction of axonal density within the same bundle's cross-section. In other words, it seems that rather than the bundle losing a number of axons but retaining its overall size, the bundles tend to shrink.

These findings are compatible with our a priori hypothesis that already in aMCI, spreading of pathological tau through WM bundles in the presence of amyloid pathology would lead to decreases in WM micro- and macrostructure that are also related to loss of synaptic density. Indeed, these findings indicate a disease-specific axonal loss. We found that quantitative amyloid burden was significantly associated with FD, FC and FDC. As previously highlighted by Dewenter et al. [62], the effect of amyloid pathology on FD might be explained by concomitant small vessel disease that was not accounted for in this study. However, the association of amyloid with fixel metrics is in agreement with previous DTI studies demonstrating WM alterations in the presence of increased amyloid burden in early AD stages [31, 68]. Moreover, single-cell transcriptomic analysis highlighted that myelination-related processes were recurrently perturbed in early AD pathology, i.e., at high amyloid burden but modest tau pathology and cognitive impairment [69].

Next, in agreement with the hypothesis postulated by McAleese et al. [70]., we found that tau pathology in connected regions was associated with FC and FDC of the connecting WM bundle. Specifically in the left hemisphere, stronger associations of FC were found with hippocampal tau compared to PCC-P tau. These findings are in line with the idea of axonal and trans-synaptic spread of tau pathology along structurally connected regions in AD [71, 72]. Interestingly, tau pathology was not significantly associated with FD changes in WM bundles, which is compatible with the idea that tau pathology specifically induces morphological WM atrophy without affecting microstructural axon density. Compared to previous DTI studies, this finding provides new insights into the effects of tau pathology on WM structural alterations, and has very recently been confirmed in a larger study [73]. Our findings are at odds with a previous study that did not find an association of tau pathology with fixel-based metrics [62]. Of note, we quantified tau pathology in regions connected by the tract-of-interest, which is different from the tau Braak stage positivity classification that was used in this previous study [62].

As for the association of fixel-based metrics with SV2A PET, we found that synaptic density in the hippocampus was associated specifically with FD but not with FC. A lack of association with PCC-P synaptic loss can be explained by the lack of SV2A group differences in this region.Importantly, the white matter region centrum semiovale was used to quantify SV2A PET data.

The reference region was created from a combined dataset of 78 HC that was available in-house. More detailed information on the creation of this reference region can be found in Michiels et al. [74] The same reference region was used for all subjects, irrespective of the presence of white matter lesions in this region in patients. Therefore, we cannot exclude the possibility that WM lesions influenced this association. To date, only one study investigated the association of structural connectivity in AD patients with SV2A PET and reported decreased structural connectivity in regions with lower synaptic density [75]. The association of SV2A PET with functional connectivity on the other hand was investigated more extensively, and studies consistently report positive associations of synaptic density with functional connectivity, either in the default-mode and executive control networks [76] or in frontal brain areas [75]. Additionally, SV2A PET has been shown to correlate with reduced functional connectivity in frontotemporal lobar degeneration [77] and in depression [78].

Interestingly, correlations of FBA metrics with PET biomarkers seemed stronger in the left hemisphere compared to the right. Upon further investigating this lateralization effect, we found that FC in the temporal cingulum bundle was not significantly different between the left and right hemisphere ($t = 1.9$; $P = 0.07$) but FD was significantly lower in the left hemisphere compared to the right ($t = 5.4$; $P < 0.0001$). However, no significant differences were present between both brain hemispheres in amyloid, tau and SV2A PET. A speculative explanation could be derived from the fact that most participants were right-handed indicating the left hemisphere to be dominant. However, further research is needed to clarify this finding.

Our study took a multimodal approach including assessments of amyloid, tau and SV2A PET and cognitive evaluations. The use of advanced techniques enabled the investigation of axonal loss with increased anatomical accuracy compared to previous voxel-based approaches. Moreover, the longitudinal study design allowed the assessment of changes in WM structure along the clinical progression of MCI to AD. As such, we extend previous findings considerably and provide useful insights for future research. Technically, the acquisition of multi-shell dMRI data allowed for the application of multi-shell multi-tissue CSD, which provides a more detailed characterization of WM microstructure compared to single-shell CSD.

However, there were a number of limitations to our study. Our sample size, especially for longitudinal assessments, was rather small which limited the power of statistical analyses. It should be noted that the correlation analyses were regarded as exploratory and therefore not corrected for multiple comparisons. However, as it is a multimodal, multitracer PET-MR study, it gives a first and integrated evaluation of hallmark parameters for early AD. Notably, we report the first longitudinal evaluation of fixel metrics in an early AD cohort. Although prevalent in AD pathology, we did not further characterize WM hyperintensities on MRI although these lesions have been shown to induce decreases in FD [62, 79]. However, as specified in the in- and exclusion criteria, we excluded HC with a Fazekas score of 3. Although WM hyperintensities visually seemed more prevalent in the aMCI group, our whole-brain FBA results demonstrate that WM macrostructural alterations as a result of axonal atrophy constitute the main effect of WM degeneration in aMCI. Additionally, these WM hyperintensities rarely encompassed the temporal cingulum bundle thereby limiting the probability for false positive findings in the tract-of-interest analysis. Next, we did not investigate the correlation of WM structural changes with gray matter atrophy. Finally, amyloid PET data were not corrected for partial volume effects.

Conclusion

In conclusion, we show widespread axonal loss already in the aMCI stage of AD that manifests to a certain extent as microstructural reductions but mostly as macrostructural WM reductions. The temporal cingulum bundle plays a central role in disease progression in AD and its structural changes are related to amyloid, tau and synaptic density alterations, in particular in the hippocampus and posterior cingulate/precuneus. Future work investigating larger patient cohorts and other WM tracts longitudinally are warranted.

Abbreviations

AAL	Automated anatomical labelling
AD	Alzheimer's disease
aMCI	Amnestic mild cognitive impairment
AVF	Animal verbal fluency
BDI	Beck's depression inventory
BNT	Boston naming test
CDR	Clinical dementia rating scale
CFE	Connectivity-based fixel enhancement
CSD	Constrained spherical deconvolution
CSF	Cerebrospinal fluid
dMRI	Diffusion-weighted MRI
DTI	Diffusion tensor imaging
FA	Fractional anisotropy
FBA	Fixel-based analysis
FC	Fibre cross-section
FD	Apparent fibre density
FDC	Fibre density and cross-section
FOD	Fibre orientation distribution
FWE	Family-wise error
FWHM	Full width at half maximum
GDS	Geriatric depression scale
HC	Healthy controls
NFTs	Neurofibrillary tangles
MCI	Mild cognitive impairment
MD	Mean diffusivity
MMSE	Mini-mental state examination
MNI	Montreal neurological institute

MSBP	MultiScale brain parcellator
OSEM	Ordered subset expectation maximization
PCC-P	Posterior cingulate cortex/precuneus
PVC	Partial volume correction
RAVLT	Rey auditory verbal learning test
RBV	Region-based voxelwise
RCPM	Raven's coloured progressive matrices
SD	Standard deviation
SPM	Statistical parametric mapping
SUV	Standardized uptake value
SUVR	Standardized uptake value ratio
SV2A	Synaptic vesicle protein 2 A
TIV	Total intracranial volume
TMT	Trail making test
VOI	Volume-of-interest
WM	White matter
ZTE	Zero-echo time

Supplementary Information

The online version contains supplementary material available at https://doi.org/10.1186/s13195-025-01710-0.

Supplementary Material 1

Acknowledgements
We thank all the participants for their willingness to participate in this study. The authors are grateful to the PET-MR technologists, in particular Kwinten Porters, Jef Van Loock and Nele Eecloo for their contribution in data acquisition. We also thank the PET radiopharmacy team and nuclear medicine medical physics team for their skilled contributions.

Author contributions
G.V. and K.V.L. were responsible for study conceptualization. G.V. and M.V. recruited study participants. G.V. performed data acquisition. G.V., A.R., J.B., D.C., S.S., M.K. and K.V.L. contributed to data analysis and interpretation. G.V. and K.V.L. drafted the manuscript, and all authors critically revised the intellectual content of the manuscript.

Funding
This study was supported by an FWO grant (FWO/G093218N) and KU Leuven internal C2 funding (C24-17-063).

Data availability
Anonymized data will be deposited in an access-controlled file server used by the academic research PET imaging group, which can be shared upon reasonable request from any qualified investigator on approval by the Ethics Committee of the local university hospital.

Declarations

Ethics approval and consent to participate
The study was approved by the local Ethics Committee UZ/KU Leuven and was conducted according to the latest version of the Declaration of Helsinki. Written informed consent was signed by all participants prior to study inclusion.

Consent for publication
Not applicable.

Competing interests
K.V.L. performed this study as senior investigator of FWO Flanders. K.V.L. is an advisory board member of Cerveau-Lantheus and has received fees through KU Leuven for consultancy activities for GE Healthcare. K.V.L. and M.K. have performed contract research through KU Leuven for Merck, Janssen Pharmaceuticals, UCB, Syndesi, Eikonizo, GE Healthcare, Cerevel, BMS and Curasen. No other potential conflicts of interest relevant to this article exist.

Author details
[1]Nuclear Medicine and Molecular Imaging, Department of Imaging and Pathology, KU Leuven, Leuven, Belgium
[2]Translational MRI, Department of Imaging and Pathology, KU Leuven, Leuven, Belgium
[3]Department of Oncology, KU Leuven, Leuven, Belgium
[4]Department of Radiology, University Hospitals UZ Leuven, Leuven, Belgium
[5]Leuven Brain Institute, Leuven, Belgium
[6]Department of Geriatric Psychiatry, University Hospitals UZ Leuven, Leuven, Belgium
[7]Neuropsychiatry, Research Group Psychiatry, KU Leuven, Leuven, Belgium
[8]Division of Nuclear Medicine, University Hospitals UZ Leuven, Leuven, Belgium

Received: 15 October 2024 / Accepted: 6 March 2025
Published online: 05 April 2025

References

1. Braak H, Braak E. Neuropathological stageing of Alzheimer-related changes. Acta Neuropathol. 1991;82(4):239–59. https://doi.org/10.1007/BF00308809
2. Thal DR, Rüb U, Orantes M, Braak H. Phases of Aβ-deposition in the human brain and its relevance for the development of AD. Neurology. 2002;58(12):1791–800. https://doi.org/10.1212/WNL.58.12.1791
3. Giorgio J, Adams JN, Maass A, Jagust WJ, Breakspear M. Amyloid induced hyperexcitability in default mode network drives medial Temporal hyperactivity and early Tau accumulation. Neuron. 2023;1–11. https://doi.org/10.1016/j.neuron.2023.11.014
4. Busche MA, Wegmann S, Dujardin S, Commins C, Schiantarelli J, Klickstein N, et al. Tau impairs neural circuits, dominating amyloid-β effects, in alzheimer models in vivo. Nat Neurosci. 2019;22:57–64. https://doi.org/10.1038/s41593-018-0289-8
5. Busche MA, Konnerth A. Impairments of neural circuit function in Alzheimer's disease. Philosophical Trans Royal Soc B: Biol Sci. 2016;371(1700). https://doi.org/10.1098/rstb.2015.0429
6. Lee WJ, Brown JA, Kim HR, La Joie R, Cho H, Lyoo CH, et al. Regional Aβ-tau interactions promote onset and acceleration of Alzheimer's disease Tau spreading. Neuron. 2022;110:1932–43. https://doi.org/10.1016/j.neuron.2022.03.034
7. Doré V, Krishnadas N, Bourgeat P, Huang K, Li S, Burnham S, et al. Relationship between amyloid and Tau levels and its impact on Tau spreading. Eur J Nucl Med Mol Imaging. 2021;48(7):2225. https://doi.org/10.1007/S00259-021-05191-9
8. Schöll M, Lockhart SN, Schonhaut DR, O'Neil JP, Janabi M, Ossenkoppele R, et al. PET imaging of Tau deposition in the aging human brain. Neuron. 2016;89(5):971–82. https://doi.org/10.1016/J.NEURON.2016.01.028
9. Vogel JW, Iturria-Medina Y, Strandberg OT, Smith R, Levitis E, Evans AC, et al. Spread of pathological Tau proteins through communicating neurons in human Alzheimer's disease. Nat Commun. 2020;11(1):2612. https://doi.org/10.1038/s41467-020-15701-2
10. Wu JW, Hussaini SA, Bastille IM, Rodriguez GA, Mrejeru A, Rilett K, et al. Neuronal activity enhances Tau propagation and Tau pathology in vivo. Nat Neurosci. 2016;19(8):1085–92. https://doi.org/10.1038/nn.4328
11. Aragão Gomes L, Andrea Hipp S, Rijal Upadhaya A, Balakrishnan K, Ospitalieri S, Koper MJ, et al. Aβ-induced acceleration of Alzheimer-related τ-pathology spreading and its association with prion protein. Acta Neuropathol. 2019;138:913–41. https://doi.org/10.1007/s00401-019-02053-5
12. Zhou L, McInnes J, Wierda K, Holt M, Herrmann A, Jackson R, et al. Tau association with synaptic vesicles causes presynaptic dysfunction. Nat Commun. 2017;8:15295. https://doi.org/10.1038/NCOMMS15295
13. McInnes J, Wierda K, Snellinx A, Bounti L, Wang Y, Stancu I, et al. Synaptogyrin-3 mediates presynaptic dysfunction induced by Tau. Neuron. 2018;97:823–35. https://doi.org/10.1016/J.NEURON.2018.01.022
14. Franzmeier N, Neitzel J, Rubinski A, Smith R, Strandberg O, Ossenkoppele R, et al. Functional brain architecture is associated with the rate of Tau accumulation in Alzheimer's disease. Nat Commun. 2020;11. https://doi.org/10.1038/s41467-019-14159-1
15. Schoonhoven DN, Coomans EM, Millán AP, van Nifterick AM, Visser D, Ossenkoppele R, et al. Tau protein spreads through functionally connected neurons

in Alzheimer's disease: a combined MEG/PET study. Brain. 2023;146(10):4040–54. https://doi.org/10.1093/brain/awad189
16. Berron D, Vogel JW, Insel PS, Pereira JB, Xie L, Wisse LEM, et al. Early stages of Tau pathology and its associations with functional connectivity, atrophy and memory. Brain. 2021;144(9):2771–83. https://doi.org/10.1093/brain/awab114
17. Hari E, Kizilates-Evin G, Kurt E, Bayram A, Ulasoglu-Yildiz C, Gurvit H, et al. Functional and structural connectivity in the Papez circuit in different stages of Alzheimer's disease. Clin Neurophysiol. 2023;153:33–45. https://doi.org/10.1016/j.clinph.2023.06.008
18. Yan S, Zheng C, Cui B, Qi Z, Zhao Z, An Y, et al. Multiparametric imaging hippocampal neurodegeneration and functional connectivity with simultaneous PET/MRI in Alzheimer's disease. Eur J Nucl Med Mol Imaging. 2020;47(10):2440–52. https://doi.org/10.1007/S00259-020-04752-8
19. Badhwar AP, Tam A, Dansereau C, Orban P, Hoffstaedter F, Bellec P. Resting-state network dysfunction in Alzheimer's disease: A systematic review and meta-analysis. Alzheimer's Dementia: Diagnosis Assess Disease Monit. 2017;8:73–85. https://doi.org/10.1016/j.dadm.2017.03.007
20. Eyler LT, Elman JA, Hatton SN, Gough S, Mischel AK, Hagler jr. Resting state abnormalities of the default mode network in mild cognitive impairment: A systematic review and Meta-Analysis. J Alzheimer's Disease. 2019;70(1):107–20. https://doi.org/10.3233/JAD-180847.Resting
21. Chao YP, Liu PTB, Wang PN, Cheng CH. Reduced Inter-Voxel white matter integrity in subjective cognitive decline: diffusion tensor imaging with Tract-Based Spatial statistics analysis. Front Aging Neurosci. 2022;14(810998). https://doi.org/10.3389/FNAGI.2022.810998
22. Veale T, Malone IB, Poole T, Parker TD, Slattery CF, Paterson RW, et al. Loss and dispersion of superficial white matter in Alzheimer's disease: a diffusion MRI study. Brain Commun. 2021;3(4):fcab272. https://doi.org/10.1093/braincomms/fcab272
23. Ramírez-Toraño F, Abbas K, Bruña R, de Pedro SM, Gómez-Ruiz N, Barabash A, et al. A structural connectivity disruption one decade before the typical age for dementia: A study in healthy subjects with family history of Alzheimer's disease. Cereb Cortex Commun. 2021;2:1–12. https://doi.org/10.1093/TEXCOM/TGAB051
24. Shafer AT, Williams OA, Perez E, An Y, Landman BA, Ferrucci L, et al. Accelerated decline in white matter microstructure in subsequently impaired older adults and its relationship with cognitive decline. Brain Commun. 2022;4(2):fcac051. https://doi.org/10.1093/braincomms/fcac051
25. Jacobs HIL, Hedden T, Schultz AP, Sepulcre J, Perea RD, Amariglio RE, et al. Structural tract alterations predict downstream Tau accumulation in amyloid-positive older individuals. Nat Neurosci. 2018;21(3):424–31. https://doi.org/10.1038/s41593-018-0070-z
26. Strain JF, Smith RX, Beaumont H, Roe CM, Gordon BA, Mishra S, et al. Loss of white matter integrity reflects Tau accumulation in alzheimer disease defined regions. Neurology. 2018;91(4):e313–318. https://doi.org/10.1212/WNL.0000000000005864
27. Kantarci K, Murray ME, Schwarz CG, Reid RI, Przybelski SA, Lesnick T, et al. White-matter integrity on DTI and the pathologic staging of Alzheimer's disease. Neurobiol Aging. 2017;56:172–9. https://doi.org/10.1016/j.neurobiolaging.2017.04.024
28. Wen Q, Risacher SL, Xie L, Li J, Harezlak J, Farlow MR, et al. Tau-related white-matter alterations along spatially selective pathways. NeuroImage. 2021;226:117560. https://doi.org/10.1016/J.NEUROIMAGE.2020.117560
29. Nabizadeh F, Pourhamzeh M, Khani S, Rezaei A, Ranjbaran F, Deravi N. Plasma phosphorylated-tau181 levels reflect white matter microstructural changes across Alzheimer's disease progression. Metab Brain Dis. 2022;37:761–71. https://doi.org/10.1007/S11011-022-00908-7
30. Carlson ML, Toueg TN, Khalighi MM, Castillo J, Shen B, Azevedo EC et al. Hippocampal subfield imaging and fractional anisotropy show parallel changes in Alzheimer's disease tau progression using simultaneous tau-PET/MRI at 3T. Alzheimer's and Dementia: Diagnosis, Assessment and Disease Monitoring. 2021;13:e12218. https://doi.org/10.1002/dad2.12218
31. Collij LE, Ingala S, Top H, Wottschel V, Stickney KE, Tomassen J, et al. White matter microstructure disruption in early stage amyloid pathology. Alzheimer's Dementia: Diagnosis Assess Disease Monit. 2021;13:e12124. https://doi.org/10.1002/dad2.12124
32. Jeurissen B, Leemans A, Tournier JD, Jones DK, Sijbers J. Investigating the prevalence of complex fiber configurations in white matter tissue with diffusion magnetic resonance imaging. Hum Brain Mapp. 2013;34:2747–66. https://doi.org/10.1002/hbm.22099
33. Seunarine KK, Alexander DC. Chapter 4: multiple fibers: beyond the diffusion tensor. in: diffusion MRI: from quantitative measurement to in vivo neuroanatomy. Academic. 2009;55–72. https://doi.org/10.1016/B978-0-12-396460-1.00006-8
34. Tournier JD, Calamante F, Connelly A. Robust determination of the fibre orientation distribution in diffusion MRI: Non-negativity constrained super-resolved spherical Deconvolution. NeuroImage. 2007;35(4):1459–72. https://doi.org/10.1016/j.neuroimage.2007.02.016
35. Raffelt DA, Tournier JD, Smith RE, Vaughan DN, Jackson G, Ridgway GR, et al. Investigating white matter fibre density and morphology using fixel-based analysis. NeuroImage. 2017;144:58–73. https://doi.org/10.1016/J.NEUROIMAGE.2016.09.029
36. Mito R, Raffelt D, Dhollander T, Vaughan DN, Tournier JD, Salvado O, et al. Fibre-specific white matter reductions in Alzheimer's disease and mild cognitive impairment. Brain. 2018;141(3):888–902. https://doi.org/10.1093/brain/awx355
37. Giraldo DL, Smith RE, Struyfs H, Niemantsverdriet E, De Roeck E, Bjerke M, et al. Investigating Tissue-Specific abnormalities in Alzheimer's disease with Multi-Shell diffusion MRI. J Alzheimer's Disease. 2022;90:1771–91. https://doi.org/10.3233/JAD-220551
38. Pascoal TA, Therriault J, Benedet AL, Savard M, Lussier FZ, Chamoun M, et al. 18F-MK-6240 PET for early and late detection of neurofibrillary tangles. Brain. 2020;143(9):2818–30. https://doi.org/10.1093/BRAIN/AWAA180
39. Vanderlinden G, Ceccarini J, Casteele T, Vande, Michiels L, Lemmens R, Triau E, et al. Spatial decrease of synaptic density in amnestic mild cognitive impairment follows the Tau build-up pattern. Mol Psychiatry. 2022;27(10):4244–51. https://doi.org/10.1038/s41380-022-01672-x
40. Albert MS, DeKosky ST, Dickson D, Dubois B, Feldman HH, Fox NC, et al. The diagnosis of mild cognitive impairment due to Alzheimer's disease: recommendations from the National Institute on Aging-Alzheimer's association workgroups on diagnostic guidelines for Alzheimer's disease. Alzheimer's Dement. 2011;7(3):270–9. https://doi.org/10.1016/j.jalz.2011.03.008
41. Nabulsi NB, Mercier J, Holden D, Carré S, Najafzadeh S, Vandergeten MC, et al. Synthesis and preclinical evaluation of 11 C-UCB-J as a PET tracer for imaging the synaptic vesicle glycoprotein 2A in the brain. J Nucl Med. 2016;57:777–84. https://doi.org/10.2967/jnumed.115.168179
42. Collier TL, Yokell DL, Livni E, Rice PA, Celen S, Serdons K, et al. cGMP production of the radiopharmaceutical [18 F]MK-6240 for PET imaging of human neurofibrillary tangles. J Label Comp Radiopharm. 2017;60:263–9. https://doi.org/10.1002/jlcr.3496
43. Schramm G, Koole M, Willekens SMA, Rezaei A, Van Weehaeghe D, Delso G, et al. Regional accuracy of ZTE-Based Attenuation correction in static [18F]FDG and dynamic [18F]PE2I brain PET/MR. Front Phys. 2019;7:211. https://doi.org/10.3389/fphy.2019.00211
44. Radwan AM, Sunaert S, Schilling K, Descoteaux M, Landman BA, Vandenbulcke M, et al. An atlas of white matter anatomy, its variability, and reproducibility based on constrained spherical Deconvolution of diffusion MRI. NeuroImage. 2022;254:119029. https://doi.org/10.1016/j.neuroimage.2022.119029
45. Mertens N, Michiels L, Vanderlinden G, Vandenbulcke M, Lemmens R, Van Laere K, et al. Impact of meningeal uptake and partial volume correction techniques on [18 F] MK-6240 binding in aMCI patients and healthy controls. J Cereb Blood Flow Metabolism. 2022;41(11):1–11. https://doi.org/10.1177/0271678X221076023
46. Betthauser TJ, Cody KA, Zammit MD, Murali D, Converse AK, Barnhart TE, et al. In vivo characterization and quantification of neurofibrillary Tau PET radioligand 18 F-MK-6240 in humans from alzheimer disease dementia to young controls. J Nucl Med. 2019;60(1):93–9. https://doi.org/10.2967/jnumed.118.209650
47. Koole M, Van Aalst J, Devrome M, Mertens N, Serdons K, Lacroix B, et al. Quantifying SV2A density and drug occupancy in the human brain using [11 C]UCB-J PET imaging and subcortical white matter as reference tissue. Eur J Nucl Med Mol Imaging. 2019;46:396–406. https://doi.org/10.1007/s00259-018-4119-8
48. Tournier JD, Smith R, Raffelt D, Tabbara R, Dhollander T, Pietsch M, et al. MRtrix3: A fast, flexible and open software framework for medical image processing and visualisation. NeuroImage. 2019;202(August):116137. https://doi.org/10.1016/j.neuroimage.2019.116137
49. Sunaert S, Radwan A. KUL NeuroImaging Suite. [cited 2024 Feb 6].
50. Veraart J, Novikov DS, Christiaens D, Ades-aron B, Sijbers J, Fieremans E. Denoising of diffusion MRI using random matrix theory. NeuroImage. 2016;142:394–406. https://doi.org/10.1016/j.neuroimage.2016.08.016

51. Kellner E, Dhital B, Kiselev VG, Reisert M. Gibbs-ringing artifact removal based on local subvoxel-shifts. Magn Reson Med. 2016;76:1574–81. https://doi.org/10.1002/mrm.26054
52. Andersson JLR, Skare S, Ashburner J. How to correct susceptibility distortions in spin-echo echo-planar images: application to diffusion tensor imaging. NeuroImage. 2003;20:870–88. https://doi.org/10.1016/S1053-8119(03)00336-7
53. Tustison NJ, Avants BB, Cook PA, Zheng Y, Egan A, Yushkevich PA, et al. N4ITK: improved N3 bias correction. IEEE Trans Med Imaging. 2010;29(6):1310–20. https://doi.org/10.1109/TMI.2010.2046908
54. Jeurissen B, Tournier JD, Dhollander T, Connelly A, Sijbers J. Multi-tissue constrained spherical Deconvolution for improved analysis of multi-shell diffusion MRI data. NeuroImage. 2014;103:411–26. https://doi.org/10.1016/j.neuroimage.2014.07.061
55. Smith RE, Tournier JD, Calamante F, Connelly A. SIFT: Spherical-deconvolution informed filtering of tractograms. NeuroImage. 2013;67:298–312. https://doi.org/10.1016/j.neuroimage.2012.11.049
56. Smith RE, Tournier JD, Calamante F, Connelly A. The effects of SIFT on the reproducibility and biological accuracy of the structural connectome. NeuroImage. 2015;104:253–65. https://doi.org/10.1016/j.neuroimage.2014.10.004
57. Genc S, Smith RE, Malpas CB, Anderson V, Nicholson JM, Efron D, et al. Development of white matter fibre density and morphology over childhood: A longitudinal fixel-based analysis. NeuroImage. 2018;183(July):666–76. https://doi.org/10.1016/j.neuroimage.2018.08.043
58. Smith RE, Dhollander T, Connelly A. On the regression of intracranial volume in Fixel-Based Analysis. In: International Society of Magnetic Resonance in Medicine. 2019;3385.
59. Raffelt DA, Smith RE, Ridgway GR, Tournier JD, Vaughan DN, Rose S, et al. Connectivity-based Fixel enhancement: Whole-brain statistical analysis of diffusion MRI measures in the presence of crossing fibres. NeuroImage. 2015;117:40–55. https://doi.org/10.1016/j.neuroimage.2015.05.039
60. Winkler AM, Ridgway GR, Webster MA, Smith SM, Nichols TE. Permutation inference for the general linear model. NeuroImage. 2014;92:381–97. https://doi.org/10.1016/j.neuroimage.2014.01.060
61. Vanderlinden G, Koole M, Michiels L, Lemmens R, Vandenbulcke M, Van Laere K. Longitudinal synaptic loss versus Tau Braak staging in amnestic mild cognitive impairment. Alzheimer's Dement. 2024;Epub ahead of print. https://doi.org/10.1002/alz.14412
62. Dewenter A, Jacob MA, Cai M, Gesierich B, Hager P, Kopczak A, et al. Disentangling the effects of Alzheimer's and small vessel disease on white matter fibre tracts. Brain. 2023;146(2):678–89. https://doi.org/10.1093/brain/awac265
63. Luo X, Wang S, Jiaerken Y, Li K, Zeng Q, Zhang R, et al. Distinct fiber-specific white matter reductions pattern in early- and late-onset Alzheimer's disease. Aging. 2021;13(9):12410–30. https://doi.org/10.18632/aging.202702
64. Hanseeuw BJ, Betensky RA, Schultz AP, Papp KV, Mormino EC, Sepulcre J, et al. Fluorodeoxyglucose metabolism associated with tau-amyloid interaction predicts memory decline. Ann Neurol. 2017;81(4):583–96. https://doi.org/10.1002/ana.24910
65. Minoshima S, Giordani B, Berent S, Frey KA, Foster NL, Kuhl DE. Metabolic reduction in the posterior cingulate cortex in very early Alzheimer's disease. Ann Neurol. 1997;42:85–94. https://doi.org/10.1002/ana.410420114
66. Berron D, van Westen D, Ossenkoppele R, Strandberg O, Hansson O. Medial Temporal lobe connectivity and its associations with cognition in early Alzheimer's disease. Brain. 2020;143:1233–48. https://doi.org/10.1093/brain/awaa068
67. Jagust WJ, Eberling JL, Richardson BC, Reed BR, Baker MG, Nordahl TE, et al. The cortical topography of Temporal lobe hypometabolism in early Alzheimer's disease. Brain Res. 1993;629:189–98. https://doi.org/10.1016/0006-8993(93)91320-R
68. Sánchez SM, Duarte-Abritta B, Abulafia C, De Pino G, Bocaccio H, Castro MN, et al. White matter fiber density abnormalities in cognitively normal adults at risk for late-onset Alzheimer's disease. J Psychiatr Res. 2020;122:79–87. https://doi.org/10.1016/j.jpsychires.2019.12.019
69. Mathys H, Davila-velderrain J, Peng Z, Gao F, Young JZ, Menon M et al. Single-cell transcriptomic analysis of alzheimer ' s disease. 2019;570:332–7. https://doi.org/10.1038/s41586-019-1195-2.Single-cell
70. McAleese KE, Walker L, Colloby SJ, Taylor JP, Thomas AJ, Decarli C, et al. Cortical Tau pathology: A major player in fibre-specific white matter reductions in Alzheimer's disease? Brain. 2018;141:e44. https://doi.org/10.1093/brain/awy084
71. Goedert M, Eisenberg DS, Crowther RA. Propagation of Tau aggregates and neurodegeneration. Annu Rev Neurosci. 2017;40:189–210. https://doi.org/10.1146/annurev-neuro-072116-031153
72. Sepulcre J, Grothe MJ, d'Oleire Uquillas F, Ortiz-Terán L, Diez I, Yang HS, et al. Neurogenetic contributions to amyloid beta and Tau spreading in the human cortex. Nat Med 2018. 2018;24(12):12. https://doi.org/10.1038/s41591-018-0206-4
73. Ahmadi K, Pereira JB, van Westen D, Pasternak O, Zhang F, Nilsson M, et al. Fixel-based analysis reveals tau-related white matter changes in early stages of Alzheimer's disease. J Neurosci. 2024;44(18):e0538232024. https://doi.org/10.1523/jneurosci.0538-23.2024
74. Michiels L, Mertens N, Thijs L, Radwan A, Sunaert S, Vandenbulcke M, et al. Changes in synaptic density in the subacute phase after ischemic stroke: A 11 C-UCB-J PET/MR study. J Cereb Blood Flow Metabolism. 2021;0(0):1–12. https://doi.org/10.1177/0271678X211047759
75. Zhang J, Wang J, Xu X, You Z. In vivo synaptic density loss correlates with impaired functional and related structural connectivity in alzheimer ' s disease. J Cereb Blood Flow Metabolism. 2023;43(6):977–88. https://doi.org/10.1177/0271678X231153730
76. Fang XT, Volpi T, Holmes SE, Esterlis I, Carson RE, Worhunsky PD. Linking resting-state network fluctuations with systems of coherent synaptic density: A multimodal fMRI and 11 C-UCB-J PET study. Front Hum Neurosci. 2023;17:1–9. https://doi.org/10.3389/fnhum.2023.1124254
77. Whiteside DJ, Holland N, Tsvetanov KA, Mak E, Malpetti M, Savulich G, et al. Synaptic density affects clinical severity via network dysfunction in syndromes associated with frontotemporal Lobar degeneration. Nat Commun. 2023;14(1):1–13. https://doi.org/10.1038/s41467-023-44307-7
78. Holmes SE, Scheinost D, Finnema SJ, Naganawa M, Davis MT, DellaGioia N, et al. Lower synaptic density is associated with depression severity and network alterations. Nat Commun. 2019;10:1529. https://doi.org/10.1038/S41467-019-09562-7
79. Dhollander T, Raffelt D, Connelly A. Towards interpretation of 3-tissue constrained spherical deconvolution results in pathology. In: 25th International Society of Magnetic Resonance in Medicine,. 2017;1815.

Publisher's note